How to cite: *Angew. Chem. Int. Ed.* **2024**, *63*, e202407817
doi.org/10.1002/anie.202407817

Noncovalent Interactions | Hot Paper

Lone-Pair-π Bond Strength Unveiled by a Combined Experimental and Computational Study

Cristian L. Gutiérrez-Peña, Ana Gutiérrez-Blanco, Dmitry G. Gusev, Macarena Poyatos, and Eduardo Peris**

Abstract: A series of naphthalene-diimide (NDI) and perylene-diimide (PDI) connected bis-N-heterocyclic carbene complexes of iridium(III) have been prepared and fully characterized. The analysis of their NMR spectroscopic features, together with their molecular structures show that these species display lone-pair-π interactions between the chloride ligands of the Ir(III) complex and the heterocycles of the NDI/PDI moieties. The detection of this type of interaction in solution is due to the formation of two atropisomers, which are formed as a result of the restricted rotation about the Ir–$C_{carbene}$ bond imposed by the (Cl)lp···π interaction. Variable-temperature ^{1}H NMR analysis allowed the determination of the strength of this non-covalent interaction, which lies between $\Delta H = 6.6$ and 10 kcal/mol. The computational studies performed fully support the experimental findings.

Introduction

Non-covalent interactions between electron-deficient aromatic systems and anions were first described by Frontera and Deyà in 2002, and were coined as anion-π interactions.[1] Soon thereafter, other two almost simultaneous reports established that these interactions are comparable in energy to cation-π interactions and moderate-strong hydrogen bonds,[2] heralding the nascence of anion-π interactions as one important subfield of supramolecular chemistry.[3] Nowadays anion-π interactions have added a new dimension to the design of selective anion receptors, colorimetric sensors, anion-π catalysts[4] and anion doping of organic semiconductors. Together with anion-π interactions, lone pair-π interactions between capped halogen atoms and electron-deficient π-systems are currently being a matter of increasing interest.[5] While this type of non-covalent interaction is well recognized in structural biology,[6] its application in catalysis has been rarely explored,[7] and its influence on the physicochemical properties in supramolecular systems is still unclear.[5e] This is very likely due to the fact that this interaction is considered to be too weak for harnessing self-assembly reactions, but most likely, because benchmark experimental and computational studies on the intrinsic strength of these non-covalent interactions are very scarce.[8]

Naphthalene-diimides (NDIs) are ideal for studying anion-π and lone pair-π interactions because their exceptionally electron-deficient parent core make them to have a strong tendency to interact with electron-rich lone-pair bearing electronegative atoms. Many groups have focused their interest towards the interaction of anions with naphthalene-diimides (NDIs), and pioneered studies towards finding key applications. For instance, Matile et al. described a bilayer formed by rigid NDI-based oligomers that mediates the transport of chlorides,[9] and Saha et al. developed a new strateofgy for toxic fluoride ion sensing.[10] We also contributed to the field, by showing how the addition of fluoride to a Rh(I) complex bearing a CNC pincer ligand functionalized with a NDI moiety facilitates the sequential one- and two-electron reduction of the NDI moiety of the ligand, thus rendering a situation in which the ligand can increase its electrondonor strength in two levels.[11] This effect had an important impact on the catalytic performance of the complex, thus revealing a new application of anion-NDI interactions to the field of homogeneous catalysis.

During the last few years, we have been particularly interested in merging the extraordinary photophysical and electrochemical properties of naphthalene-diimides (NDIs)[12] with those of N-heterocyclic carbene (NHC) ligands. We first designed a series of NDI-NHC ligands, and demonstrated that their corresponding complexes could be successfully employed as redox-switchable catalysts in the cycloisomerization of alkynoic acids[13] and the hydroamination of acetylenes.[14] Our studies revealed that the redox-switchable character of the NDI fragment allows the modification of the electron-donating strength of the final NDI-NHC ligands in a controlled and reversible manner.

[*] C. L. Gutiérrez-Peña, Dr. A. Gutiérrez-Blanco, Dr. M. Poyatos, Prof. E. Peris
Institute of Advanced Materials (INAM). Universitat Jaume I
Av. Vicente Sos Baynat s/n. Castellón. E-12071. Spain
E-mail: poyatosd@uji.es
eperis@uji.es
Prof. D. G. Gusev
Department of Chemistry and Biochemistry, Wilfrid Laurier University, 75 University Avenue West, Waterloo, Ontario, N2 L3 C5 Canada

Built on these grounds, we now report a series of dimetallic di-N-heterocyclic carbene complexes of iridium connected by a di-propyl-NDI linker, and show how these complexes display important lone pair-π interactions between the chloride ligands and the NDI moiety of the linker. This type of interaction is clearly manifested both in the solid state and in solution, and we will show how the energy of this interaction is stronger than has been thought so far.

Results and Discussion

For the preparation of the dimetallic Cp*Ir(III) complexes we used the imidazolium salts [**1A**]$(BF_4)_2$ and [**1B**]$(Br)_2$, which we reported previously.[15] The preparation of the complexes was performed by transmetallation of the NHC ligands from the in situ preformed silver-NHC complexes, following the procedure shown in Scheme 1. The resulting complexes **2A** and **2B** were obtained as orange solids, in 40 and 64 % yields, respectively. Both complexes were characterized by NMR spectroscopy and mass spectrometry and gave satisfactory elemental analysis. Contrary to what we had expected, the ^{1}H NMR spectra of **2A** and **2B** showed the presence of two species in solution. This was evidenced by the appearance of two sets of signals due to the protons of the NDI core, and also due to the protons of the methyl groups of the Cp* ligands, together with the appearance of two pairs of doublets assigned to the protons at the backbone of the NHC ligands (see ESI for full details). The diffusion-ordered NMR spectrum (DOSY) of **2B** showed only one diffusion coefficient, indicating that the two species present in solution had the same (or very similar) hydrodynamic radii. This, together with the fact that samples of **2B** gave satisfactory elemental analyses considering the molecular formula assumed for **2B**, made us conclude that the species present in solution of these two complexes were isomers. As will be discussed below, a VT ^{1}H NMR experiment using **2B** showed that its two isomers are interconverting, thus explaining why their separation in solution is not possible. The integration of the ^{1}H NMR resonances indicated a 2/1 molar ratio of the two isomers in **2A**, and 1/1 in **2B** for their solutions in deuterated tetrachloroethane.

The removal of the chloride ligands in **2B** was performed by adding four equivalents of silver triflate to a solution of the complex in acetonitrile. A ^{1}H NMR spectrum of the resulting complex (**3B**) showed the pattern expected for a single species, as it displayed one singlet due to the four equivalent protons of the NDI core, one singlet of all protons of the methyl groups of the Cp* ligands, and two doublets due to the protons of the backbone of the NHC ligands. This experiment indicated that the nature of the two isomers observed for **2B** (and **2A**), is very likely due to the presence of the chloride ligands. Complex **3B** was further characterized by means of ^{13}C NMR spectroscopy and mass spectrometry.

The addition of two equivalents of silver triflate to a solution of **2B** in CH_2Cl_2 followed by bubbling of carbon monoxide, resulted in formation of **4B**, a complex bearing one chloride ligand and one carbonyl in each iridium fragment. This complex was characterized by means of NMR spectrometry and mass spectrometry. The ^{1}H NMR spectrum of **4B** indicated the presence of only one species, as a single resonance was observed for the four equivalent protons of the NDI moiety. The infrared spectrum of a dichloromethane solution of **4B** exhibited the C–O stretching band at 2050 cm^{-1}.

When compound **2A** reacted with two equivalents of silver tetrafluoroborate in DMSO, yellow crystals of the dicationic complex **5A** were obtained. This complex could not be characterized by ordinary spectroscopic means due to its insolubility in most organic solvents, but single crystal X-ray diffraction studies allowed us to determine its molecular structure (see below for details).

The molecular structures of complexes **2B** and **5A** were confirmed by means of single crystal X-ray diffraction studies.[16] The structure of **2B** consists of two Cp^*IrCl_2 moieties bridged by the bis-NHC-NDI ligand. The Ir–$C_{carbene}$ bond is 2.071(19) Å long (Figure 1). The two Cp^*IrCl_2 fragments are arranged on the opposite sides of the NDI plane in **2B**. Interestingly, in each iridium fragment, one chloride ligand is pointing toward the NDI moiety. The closest distance from this chloride to the NDI plane is 3.32 Å, thus in the range of chloride lone pair-π [Cl(lp)···π] interactions, which typically occur at distances from 3.22 to 3.45 Å.[5b] This situation renders a structure in which each of the Cp* ligands bound to the iridium atoms are disposed in an *anti*-conformation relative to each other. The molecular structure of **5A** is very similar to that shown for **2B** with the difference that one of the chloride ligands in each Cp*Ir moiety is replaced by a molecule of dimethyl sulfoxide (DMSO). This makes the complex to be dicationic (two BF_4^- anions are also observed in the structure). The distance of the Ir–$C_{carbene}$ bond is 2.081(11) Å. Again, the chloride ligands are pointing towards the NDI moiety. The distance between the chloride ligand and the NDI plane is 3.40 Å, also in the range of distances typically observed for Cl(lp)···π interactions.

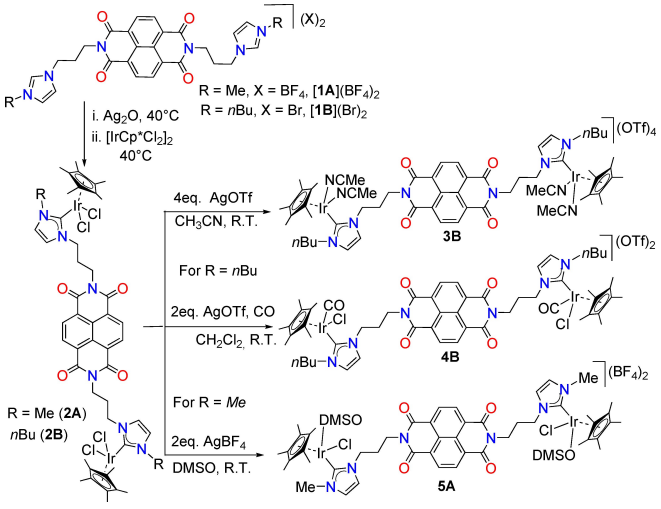

Scheme 1. Synthesis of NDI-linked di-Ir(III)Cp* complexes

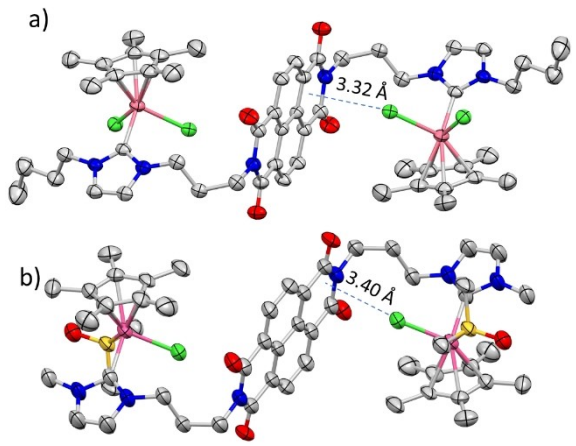

Figure 1. Molecular structures of **2B** (a) and **5A** (b) obtained from single-crystal diffraction studies. Hydrogen atoms and molecules of solvent are omitted for clarity. The BF_4 counter anions are also omitted in **5A**. Carbon atoms are in grey, nitrogen in blue, oxygen in red, iridium in magenta and sulfur in orange.

Once the molecular structures of **2B** and **5A** were established, we wondered whether the two isomers observed in solutions of **2A** and **2B** could differ by the relative configurations of the Cp*$IrCl_2$ fragments. Depending on which of the two chloride ligands is interacting with the NDI moiety, we would have two different orientations of the Cp* ligand with respect to the NDI fragment. In a monometallic complex this should remain unnoticed, but in a dimetallic complex like **2** the two possible orientations of the Cp* ligands would result in two distinct structures (atropisomers) where the Cp* ligands are either on the same side (*syn*-conformation) or on the opposite sides (*anti*-conformation) *vs.* the NDI, as shown in Figure 2.

The fact that the ^{1}H NMR spectra of **2A** and **2B** show separate resonances for each atropisomer suggests slow kinetics on the NMR timescale for the **2**(*anti*) ↔**2**(*syn*) equilibrium. To shed some light on this dynamic process, a variable temperature ^{1}H NMR experiment was performed in $C_2D_2Cl_4$, with temperatures ranging from 303 to 353 K. As can be observed from the series of spectra shown in Figure 3a, the signals due to both isomers start to broaden

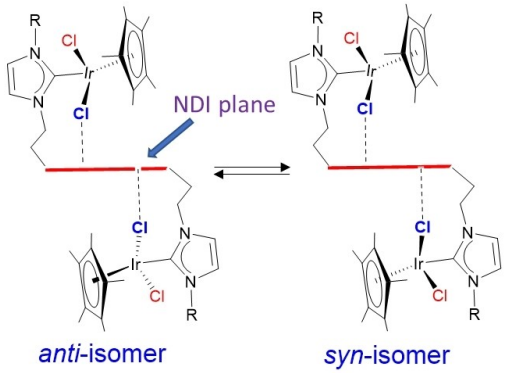

Figure 2. Schematic view of the two atropisomers of **2**.

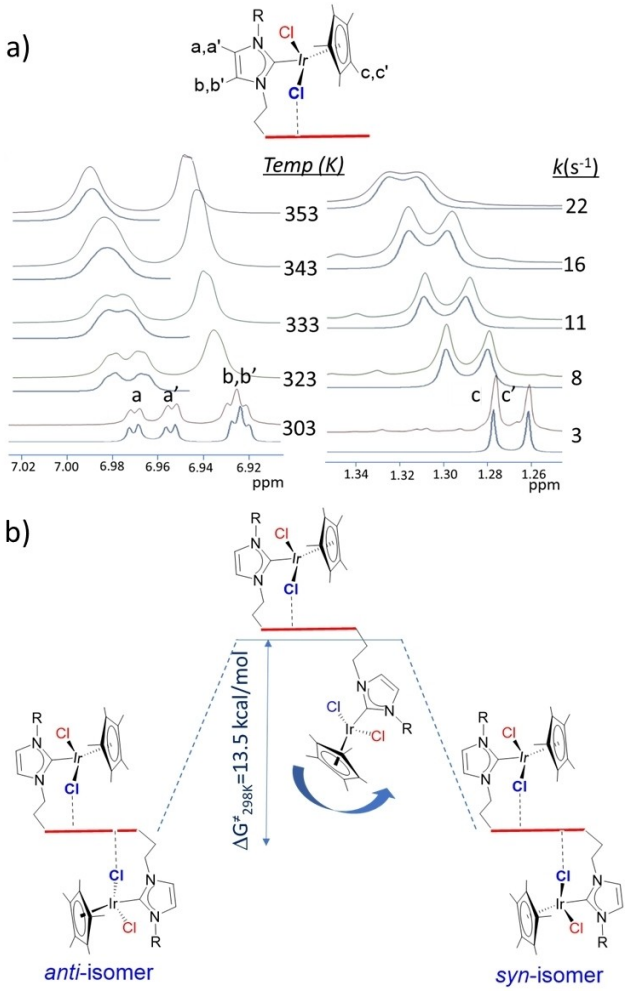

Figure 3. a) Study of the dynamic behaviour of complex **2B** investigated by variable-temperature ^{1}H NMR spectroscopy. All spectra recorded in $C_2D_2Cl_4$. The determination of the kinetic constants was performed by dynamic ^{1}H NMR simulations using SpinWorks 4.0. The simulated NMR spectra are shown below the experimental ones. b) Schematic kinetic profile of the dynamic equilibrium between atropisomers **2B**(*anti*) and **2B**(*syn*).

as the temperature increases, indicating an exchange between the two isomers. ^{1}H NMR line-shape simulations of the spectra of Figure 3 allowed us to estimate the exchange rate constants at different temperatures. An Eyring plot was used to derive the $\Delta H^{\neq}$ and $\Delta S^{\neq}$ values, which were 8.3 ± 0.2 kcal/mol and -17.4 ± 0.5 cal/molK, respectively, so that the activation Gibbs energy for the interconversion of the two isomers at room temperature is determined to be $\Delta G^{\neq}_{298K} = 13.5$ kcal/mol. For this dynamic exchange, the enthalpy cost to form the transition state should mainly arise from the cleavage of the Cl(lp)···π interaction, thus we can consider that this enthalpy value is an approximate estimation of the strength of this non-covalent interaction. The large and negative entropy cost indicates that the transition state is more solvated than the ground state, as should be expected for this intramolecular dissociative process

Structures of the two atropisomers of **2** have been optimized using DFT calculations on **2A**, and the resulting geometries are presented in Figure 4. The minor (*syn*) isomer of **2A** is less favorable by $\Delta H = 0.6$ kcal/mol. The Gibbs energy difference between the *anti* and *syn* atropisomers is $\Delta G = 1.1$ kcal/mol, in a reasonable agreement with the experimental value, $\Delta G = 0.4$ kcal/mol. The main (*anti*) isomer of **2A** has a structure closely resembling that of **2B** in Figure 1. The minor isomer of **2A** can be viewed as a product of rotation around the C–C and C–Ir bonds 1 and 2, respectively, as indicated in Figure 4. The N–C–C–C dihedral angle around bond 1 changes from 65.1° in the *anti* to −63.9° in the *syn* isomer. Changes in the dihedral angles around the next two bonds toward the NHC fragment are negligible. A significant rotation happens about bond 2; e.g., the $N–C_{(carbene)}–Ir–Cl4$ angle changes from −53.1° in the *anti* to 137.2° in the *syn* isomer. As a result, the Cp^*IrCl_2 fragment is flipped, and the two Cp* ligands are *syn* in the minor isomer (that is, the Cp* ligands are pointing towards the same side in Figure 4).

Although no symmetry has been enforced during the calculations, the optimized geometries of the major and minor isomers of **2A** possess C_i and C_2 symmetries, respectively. Thus, the iridium fragments are related by symmetry and are structurally equivalent in each isomer. A single set of NMR resonances and chemical shifts is expected for the two iridium fragments of the *anti*-isomer, as well as for the *syn* isomer of **2A**. The closest distance of the chlorides to the NDI fragment is 3.28 Å in **2A**, similar to the experimental value of 3.40 Å for **2B**.

An examination of the structure of **2A** suggests that between the two rotations - about bonds 1 and 2 - the latter is less likely to take place first for steric reasons, because of the proximity of the bulky Cp^*IrCl_2 fragment to the NDI fragment. It is more likely that rotation about bond 1 happens first, as shown in Figure 3, followed by rotation about bond 2 (with some adjustments in the angles of the bonds between bond 1 and 2). Our DFT calculations established that rotation about bond 1 leads to a transition state at $\Delta H^{‡} = 10.1$ kcal/mol ($\Delta G^{‡} = 11.6$ kcal/mol). The calculated $\Delta G^{‡}$ is in a reasonable agreement with the experimental isomerization barrier of 13.5 kcal/mol for **2B** (Figure 3). From the transition state, continued rotation about bond 1 leads toward an unstable intermediate which structure is shown in Figure 5, at $\Delta H = 9.1$ kcal/mol ($\Delta G =$ 8.0 kcal/mol). One close Ir–Cl···NDI interaction that was present in the *anti* isomer is lost in the intermediate of Figure 5. When considering the structure of this intermediate, it is apparent that the Cp^*IrCl_2 fragment that has been rotated away from the NDI moiety is not sterically constrained. Also, the three-carbon atom chain connecting the rotated iridium fragment with the central NDI moiety is linear and not strained. Thus, the reason for the intermediate of Figure 5 to have a higher energy *vs.* the main isomer of **2A** should be attributed to the loss of one Cl(lp)···π interaction. On the basis of this consideration, the calculated $\Delta H = 9.1$ kcal/mol can be viewed as a close estimate of the enthalpy of the Cl(lp)···π interaction in **2A**.

To explore if we could detect the same type of Cl(lp)···π interaction using a different electron-deficient π-system, we decided to obtain the perylene-diimide bis-NHC iridium (III) complex **7B**. The synthesis of complex **7B** was performed in a similar manner as that for **2B**, but using the perylene-functionalized bis-imidazolium salt $[\mathbf{6B}](I)_2$, as shown in Scheme 2. Complex **7B** was characterized by means of NMR spectroscopy and mass spectrometry. As happened with **2B**, the ^1H NMR ($C_2D_2Cl_4$) spectrum of **7B** showed a pattern of signals that indicated the existence of two atropisomers. In this case, the relative molar ratio between the two isomers was 2/3. The dynamic interconversion of the two atropisomers was studied by variable temperature ^1H NMR spectroscopy using a temperature range between 303 and 353 K (see ESI for full details). ^1H NMR line-shape simulations of the spectra allowed us to calculate the kinetic constants at each temperature. The

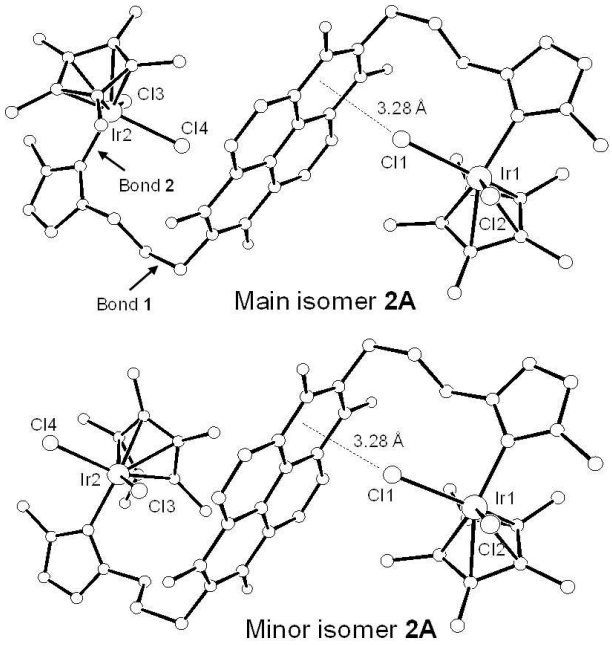

Figure 4. The structures of atropisomers of **2A** calculated using the MN15-L/def2-TZVP (def2-QZVP for Ir) method, in the solvent continuum of CH_2Cl_2 (the hydrogen atoms are not shown).

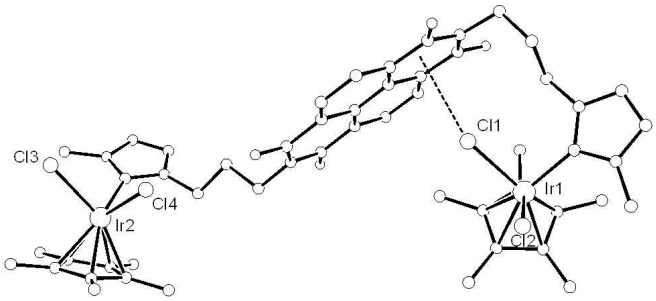

Figure 5. The structure of an unstable intermediate in the isomerization of **2A**, calculated using the MN15-L/def2-TZVP (def2-QZVP for Ir) method, in the solvent continuum of CH_2Cl_2 (the hydrogen atoms are not shown).

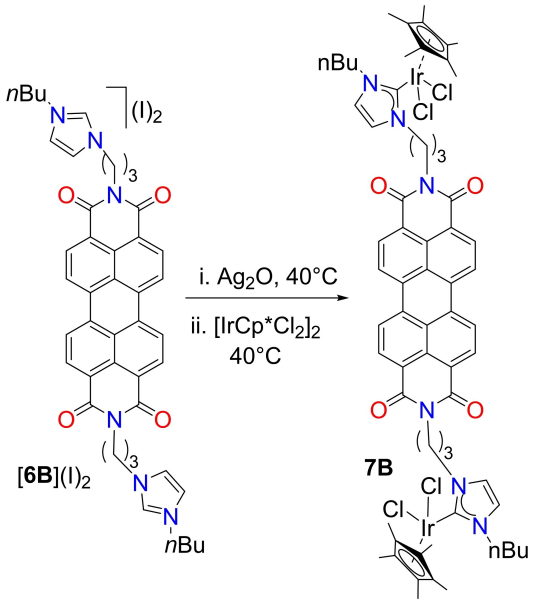

Scheme 2. Synthesis of the perylene-diimide (PDI) bis-NHC complex **7B**.

$\Delta H^{\neq}$ and $\Delta S^{\neq}$ values obtained from the corresponding Eyring plot were 6.6 ± 0.2 kcal/mol and -21.3 ± 0.7 cal/molK, respectively, and thus the activation Gibbs energy for interconversion of the two atropisomers at room temperature is $\Delta G^{\neq}_{298K} = 12.7$ kcal/mol, very similar to that observed for **2B**.

In order to give further support to our study, we also synthesized a monometallic Cp*Ir(III)-based complex bearing an NDI-functionalized NHC ligand. This complex (**9**, as shown in Figure 6), was obtained from the corresponding NDI-functionalized imidazolium salt, [**8**](I), using a synthetic protocol similar to that shown for the dimetallic complexes shown in Scheme 1 (see ESI for full details). Complex **9** was characterized by means of NMR spectroscopy, and the complete assignation of the resonances was performed by combining 2-dimensional ^{1}H–^{1}H and ^{1}H–^{13}C correlations. As expected, the ^{1}H NMR spectrum of the complex in $CDCl_3$ shows two doublets assigned to the hydrogens at the backbone of the imidazolylidene ring, and one singlet due to the 15 equivalent protons of the Cp* ligand (See ESI for details). This indicates that only one species is present in solution, as no isomers should be expected here. However, the region that shows the resonances due to the protons of the methylene groups bound to nitrogen (3.5–5.3 ppm), shows that all three N-methylene groups show diasterotopic protons, a situation that can be explained if a rigid cyclic structure arising from a non-covalent Cl(lp)···π(NDI) interaction is produced, as it is depicted in Figure 6. If this interaction was not present in solution, then both protons from the same N–CH_2 groups should appear as equivalent, as the rotation about the $C_{carbene}$–Ir bond should be fast on the NMR timescale in the structure lacking of the Cl(lp)···π-(NDI) interaction.

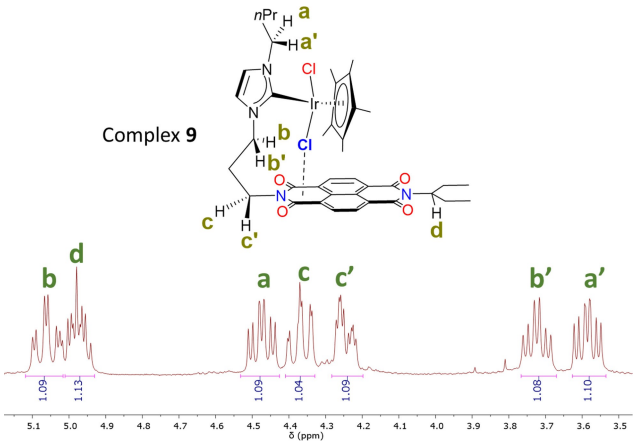

Figure 6. A drawing of complex **9**, and the region of the ^{1}H NMR spectrum ($CDCl_3$) showing the resonances of the N–CH_2 protons.

Conclusion

In summary, we obtained a series of NDI and PDI-functionalized di-NHC complexes of iridium (III) and found clear evidence of lp···π interaction between the chloride ligands of the metal and the electron deficient NDI or PDI linkers of the di-NHC ligands. This non-covalent lp···π interaction is manifested both in the solid state and in solution. The VT ^{1}H NMR analysis of two of the complexes allowed us to estimate the enthalpy of the interaction, which ranges from 6.6 (for the interaction with PDI) to 8.3 kcal/mol (for the interaction with NDI). This result is in agreement with the estimated value of the lp···π interaction enthalpy of 9.1 kcal/mol from the DFT calculations. The range of enthalpies found suggests that the energy of this type of non-covalent interaction lies among the largest found for other reported lp···π interactions.[5g,7a] An important feature of our study is that we were able to detect this type of interaction in solution due to the formation of two atropisomers, which are formed as a result of the restricted rotation imposed by the lp···π interaction. It needs to be mentioned that a monometallic complex, or a dimetallic complex bearing only one halide ligand per metal (and thus only one possible orientation of the metal fragment with respect to the NDI/PDI plane) would have made this interaction unnoticed in solution. To the best of our knowledge, our study represents the first rigorous combined spectroscopic/computational determination of the lp···π interaction. The use of NDI/PDI-moieties coupled with halogen containing metal complexes can be extended to a wide variety of a lp···π bonded complexes, and this paves the way for studying in detail what factors are dictating the strength of this type of interaction.

We also think that this non-covalent interaction may be important for inducing long range electronic effects from the NDI core to the metal. In fact, we already observed this effect in a previously published work. We recently published one study in which the same NDI-containing ligand used for the preparation of **2B** was coordinated to RhCl(COD) and

$RhCl(CO)_2$.[13b] The molecular structure of the NDI-[NHC-$RhCl(COD)]_2$ complex indicated the existence of a clear Cl(lp)···π interaction, but we did not recognize it then. Interestingly, the electrochemical reduction of the NDI core on the NDI-[NHC-$RhCl(CO)_2]_2$ complex resulted in the significant decrease of the stretching frequency of the CO ligands, therefore indicating that the reduction of the NDI core resulted in a significant increase of the electronrichness of the metal. This observation, which we were unable to explain due to the 'apparent' electronic disconnection between the NDI core and the metal, becomes now clear as the electronic connection is very likely produced through the lp···π interaction, therefore highlighting the great potential that this long-range interaction may have in future design of homogeneous catalysts.

Supporting Information

The Supporting Information file contains all the experimental and computational details dealing with the characterization of the new complexes, and X-ray diffraction details. This includes all NMR spectra, and description of methods for determining the observed kinetic constants and thermodynamic parameters.

The authors have cited additional references within the Supporting Information.[17]

Acknowledgements

We gratefully acknowledge financial support from the Ministerio de Ciencia y Universidades (PID2021-127862NB-I00 and TED2021-130647B-I00) and the Universitat Jaume I (UJI-B2021-39). A.G.B wants to acknowledge the Ministerio de Universidades, supported by the Margarita Salas postdoctoral contract MGS/2022/02(UP2021-021). We are grateful to the Serveis Centrals d'Instrumentació Científica (SCIC-UJI) for providing with spectroscopic facilities.

Conflict of Interest

The authors declare no conflict of interest.

Data Availability Statement

The data that support the findings of this study are available in the supplementary material of this article.

Keywords: Supramolecular Chemistry · non-covalent interactions · N-heterocyclic carbene · iridium · naphthalene-diimides

[1] D. Quinonero, et al., *Angew. Chem. Int. Ed.* **2002**, *41*, 3389–3392.
[2] a) M. Mascal, A. Armstrong, M. D. Bartberger, *J. Am. Chem. Soc.* **2002**, *124*, 6274–6276; b) I. Alkorta, I. Rozas, J. Elguero, *J. Am. Chem. Soc.* **2002**, *124*, 8593–8598.
[3] a) I. A. Rather, S. A. Wagay, R. Ali, *Coord. Chem. Rev.* **2020**, *415*, 213327; b) H. T. Chifotides, K. R. Dunbar, *Acc. Chem. Res.* **2013**, *46*, 894–906; c) B. L. Schottel, H. T. Chifotides, K. R. Dunbar, *Chem. Soc. Rev.* **2008**, *37*, 68–83.
[4] M. A. G. Lopez, M. L. Tan, A. Frontera, S. Matile, *JACS Au* **2023**, *3*, 1039–1051.
[5] a) M. Egli, S. Sarkhel, *Acc. Chem. Res.* **2007**, *40*, 197–205; b) T. J. Mooibroek, P. Gamez, J. Reedijk, *CrystEngComm* **2008**, *10*, 1501–1515; c) X. Fang, X. Yuan, Y. B. Song, J. D. Wang, M. J. Lin, *CrystEngComm* **2014**, *16*, 9090–9095; d) A. Bauzá, T. J. Mooibroek, A. Frontera, *ChemPhysChem* **2015**, *16*, 2496–2517; e) J. J. Liu, et al., *Dalton Trans.* **2015**, *44*, 17312–17317; f) J. J. Liu, et al., *Dalton Trans.* **2015**, *44*, 653–658; g) J. Novotny, S. Bazzi, R. Marek, J. Kozelka, *Phys. Chem. Chem. Phys.* **2016**, *18*, 19472–19481.
[6] H. Kruse, K. Mrazikova, L. D'Ascenzo, J. Sponer, P. Auffinger, *Angew. Chem. Int. Ed.* **2020**, *59*, 16553–16560.
[7] a) H. Hao, X. T. Qi, W. P. Tang, P. Liu, *Org. Lett.* **2021**, *23*, 4411–4414; b) A. J. Neel, A. Milo, M. S. Sigman, F. D. Toste, *J. Am. Chem. Soc.* **2016**, *138*, 3863–3875.
[8] C. S. Anstoter, J. P. Rogers, J. R. R. Verlet, *J. Am. Chem. Soc.* **2019**, *141*, 6132–6135.
[9] V. Gorteau, G. Bollot, J. Mareda, A. Perez-Velasco, S. Matile, *J. Am. Chem. Soc.* **2006**, *128*, 14788–14789.
[10] a) S. Guha, F. S. Goodson, L. J. Corson, S. Saha, *J. Am. Chem. Soc.* **2012**, *134*, 13679–13691; b) S. Guha, et al., *J. Am. Chem. Soc.* **2011**, *133*, 15256–15259; c) S. Guha, S. Saha, *J. Am. Chem. Soc.* **2010**, *132*, 17674–17677.
[11] S. Martínez-Vivas, D. G. Gusev, M. Poyatos, E. Peris, *Angew. Chem. Int. Ed.* **2023**, *62*, e202313899.
[12] S. V. Bhosale, et al., *Chem. Soc. Rev.* **2021**, *50*, 9845–9998.
[13] a) C. Ruiz-Zambrana, A. Gutierrez-Blanco, S. Gonell, M. Poyatos, E. Peris, *Angew. Chem. Int. Ed.* **2021**, *60*, 20003–20011; b) C. L. Gutierrez-Pena, M. Poyatos, E. Peris, *Chem. Commun.* **2022**, *58*, 10564–10567.
[14] C. Ruiz-Zambrana, M. Poyatos, E. Peris, *ACS Catal.* **2022**, *12*, 4465–4472.
[15] C. Gutiérrez-Peña, M. Poyatos, E. Peris, *Organometallics* **2023**, *42*, 1487–1494.
[16] DepoDeposition numbers 2349567 (for **2B**), 2349569 (for **5B**) contain the supplementary crystallographic data for this paper. These data are provided free of charge by the joint Cambridge Crystallographic Data Centre and Fachinformationszentrum Karlsruhe Access Structures service.
[17] a) A. Kalita, et al., *ACS Appl. Mater. Interfaces* **2016**, *8*, 25326–25336; b) P. K. R. Panyam, T. Gandhi, *Adv. Synth. Catal.* **2017**, *359*, 1144–1151; c) T. Fujiyama, K. Sugimoto, S. Michuri, *EP1736476 A1* **2006**; d) C. White, A. Yates, P. M. Maitlis, *Inorg. Synth.* **1992**, *29*, 1144–1151; e) O. V. Dolomanov, L. J. Bourhis, R. J. Gildea, J. A. K. Howard, H. Puschmann, *J. Appl. Crystallogr.* **2009**, *42*, 339–341; f) L. Palatinus, J. Prathapa, S. van Smaalen, *J. Appl. Crystallogr.* **2012**, *45*, 575–580; g) P. Vandersluis, A. L. Spek, *Acta Crystallogr. Sect. A* **1990**, *46*, 194–201; h) M. J. Frisch, et al., *Gaussian 16*, *Revision C.01*, Gaussian, Inc., Wallinford, CT, **2016**; i) H. S. Yu, X. He, D. G. Truhlar, *J. Chem. Theory Comput.* **2016**, *12*, 1280–1293; j) A. V. Marenich, C. J. Cramer, D. G. Truhlar, *J. Phys. Chem. B* **2009**, *113*, 6378–6396; k) F. Weigend, *Phys. Chem. Chem. Phys.* **2006**, *8*, 1057–1065; l) F. Weigend, R. Ahlrichs, *Phys. Chem. Chem. Phys.* **2005**, *7*, 3297–3305.

Manuscript received: April 24, 2024
Accepted manuscript online: May 15, 2024
Version of record online: June 30, 2024